Advanced parametric study of three-pinned steel arches

Matheus M. Oliveira, Jackson S. Rocha Segundo, Iara S. Azevedo, Ricardo A.M. Silveira, Arlene M.C. Sarmanho, Andrea R.D. Silva

Dept. of Civil Engineering, Federal University of Ouro Preto
Morro do Cruzeiro, 35400-000, Ouro Preto/MG, Brazil
matheus.miranda@aluno.ufop.edu.br, jackson.segundo@aluno.ufop.edu.br, iara.azevedo@aluno.ufop.edu.br, ricardo@ufop.edu.br, arlene@ufop.edu.br, andreardsilva@ufop.edu.br

Abstract. The arches are structural elements widely used from antiquity to the present times, since these elements generally present an increase in rigidity due to their curvature, outstanding in the use of drainage structures and vaults. Arches are characterized by a strongly nonlinear behavior, being an important target of study to know the structural behavior and to guarantee reliability and safety of structures that have such an element. Thus, this work focuses on the parametric study of three-pinned arches with physical and geometric nonlinearities. To investigate the complete behavior, first-order elastic (FOE), second-order elastic (SOE), first-order inelastic (FOI) and second-order inelastic (SOI) analyses are performed using the computer software MASTAN2. Therefore, the influence of the geometric and physical parameters, the arch's shape, the boundary conditions, and the stiffness of three-pinned arches are evaluated. The results obtained indicate under which conditions the arches present the better behavior performance in terms of stability and resistance.

Keywords: three-pinned arch, advanced analysis, steel, structural nonlinear response.

1 Introduction

Due to their curvature, which introduces strength gains, arches have always been widely used as structural elements. Intuitively and empirically, primitive societies used these elements to bridge extensive gaps and create wider unobstructed areas. Allied to the absence of tensile-resistant materials, arches became the basis of European architecture being widely used during the Roman period, since the compression and bending efforts are predominant in this type of element.

Despite the structural advantages, arches usually present a strongly nonlinear structural behavior, coming from different sources, with emphasis on geometry (due to large displacements), material (inelastic behavior), and semi-rigid supports. Thus, the parametric study of the influence of the main parameters of an advanced analysis becomes essential for a better understanding of the behavior of these elements.

Therefore, the present research aims at the advanced parametric study of these arches through computational finite element (FE) modeling via the computer software MASTAN2. The behavior of three-pinned arches was evaluated considering geometric and physical nonlinearities, through first-order elastic (FOE) and second-order elastic (SOE) analyses, and first-order inelastic (FOI) and second-order inelastic (SOI) analyses. Thus, the influence of geometric and physical parameters, arch's shape, boundary conditions, and stiffness of the three-pinned arches are evaluated on this article.

2 Numerical formulations

The computer system MASTAN2 [1] can be described as a program for advanced analysis of two- or three-dimensional frames and trusses subjected to static loads. The analysis routines provide options for elastic and inelastic first or second-order analyses [2].

Considering a displacement finite element formulation, for linear elastic structural analysis, it is necessary to build the elastic stiffness matrix, $\mathbf{K}_e$, and the problem can be solved according to:

$$\boldsymbol{K}_e \boldsymbol{U} = \boldsymbol{P} \tag{1}$$

where **U** is the nodal displacements vector and **P** is the nodal load vector. For higher levels, the nonlinear equilibrium equations are solved using numerical techniques and taking an incremental form of Eq. (1), as showed below:

$$\boldsymbol{K}_t \Delta \boldsymbol{U} = \Delta \boldsymbol{P} \tag{2}$$

where $\mathbf{K}_t$ is the tangent stiffness matrix, $\Delta\mathbf{U}$ is the nodal incremental displacements vector, and $\Delta\mathbf{P}$ is the nodal incremental load vector and reactions. The matrix $\mathbf{K}_t$ has a linear elastic component and one or more additional components that are functions of the internal forces and/or displacements existing at the beginning of the external load increment. This structural computational problem is well established for obtain the unknown incremental displacement vector and to determine in sequence the internal finite elements forces, making this in a gradual way, in which the total answer is determined through the sum of the increments.

In second-order elastic analysis, the deformations and finite displacements effects are accounted for in the formulation of the equilibrium equations and Eq. (2) becomes:

$$\left[\boldsymbol{K}_e + \boldsymbol{K}_g \right] \Delta \boldsymbol{U} = \Delta \boldsymbol{P} \tag{3}$$

where $\mathbf{K}_g$ is the geometric stiffness matrix, which represents the change in stiffness that results from these effects.

In first-order inelastic analysis, the algebraic equilibrium equations are defined considering the undeformed structure configuration, and Eq. (2) is rewritten as:

$$\left[\boldsymbol{K}_e + \boldsymbol{K}_m \right] \Delta \boldsymbol{U} = \Delta \boldsymbol{P} \tag{4}$$

where the matrix $\mathbf{K}_m$ represents the change coming from the inelastic behavior of the structural system. In second-order inelastic analysis, the nonlinear geometric and material parameters are considered, and the structural equilibrium equations can be written according to [3]:

$$\left[\boldsymbol{K}_e + \boldsymbol{K}_g + \boldsymbol{K}_m \right] \Delta \boldsymbol{U} = \Delta \boldsymbol{P} \tag{5}$$

3 Numerical Analysis

For the development of the numerical models, a statically determined three-pinned arch was considered under a radially distributed load q, with translations restricted and rotation permitted at the arch ends. Figure 1presents a scheme of the geometry of the complete arch and a simplified scheme of half of the arch. The physical and geometric data of a steel arch studied by Pi and Bradford [4] were used and are detailed in Tab.1. The radial load q was determined according to:

$$q = N_{E2} R \tag{6}$$

in which $N_{E2} = \pi^2 EI/(S/2)^2$ is the second buckling mode and R is the arch radius. The method applied to solve the nonlinear problem was the predictor-corrector and all load increments were $0.001qR/N_{E2}$.

The model mesh and typology, full arch (FA) and half arch (HA), studies were carried out to obtain satisfactory results and reduce the computational time. It was observed that the HA model with 10 elements presented small differences compared to a more refined one, and this model was chosen for the most of the analyses. Figure 2 shows the three-pinned arch equilibrium paths obtained through FOE and SOE analyses, and also through the analytical formulations presented by Pi and Bradford [4] for $2\theta = 45.8°$ and $2\theta = 22.9°$. For both analyses, it was possible to observe the similarity of the results. In the Figure 2, see that the x-axis and y-axis represent the variations of the dimensionless central radial displacement (v/f) and of the dimensionless radial load (qR/N_{E2}), respectively.

Figure 3 shows the equilibrium paths for the 4 analyses (FOE, SOE, FOI, and SOI), and it can be observed

that the limit load obtained through the second-order inelastic (SOI) analysis, considering non-linear physical and geometric effects, has the lowest value. Therefore, the need to evaluate the three-pinned arch (2θ = 45,8°) behavior considering different sources of nonlinearity is evident.

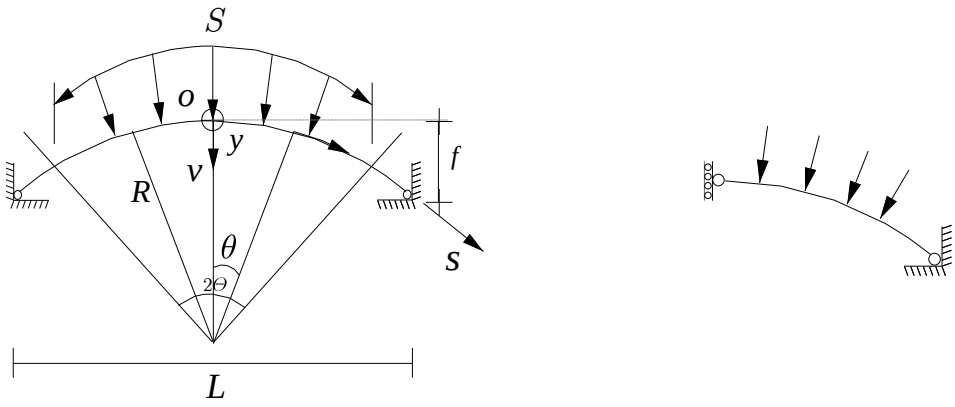

Figure 1. Three-pinned arch: the complete arch geometry and the simplified arch geometry scheme (half arch)

Table 1. Three-pinned arch data from Pi and Bradford [4]

Pi and Bradford Arch (2015)	**EI (kNm²)**	**2θ (°)**	**Radius (R) (m)**	**Arc Lenght (S) (m)**	**N_{E2} (kN)**	***q* (kN/m)**
	11154	45.8	13.51	10.8	3775.23	279.42287
E – Young's modulus I – Second moment of area				N_{E2} - Euler's critical load of 2º mode		

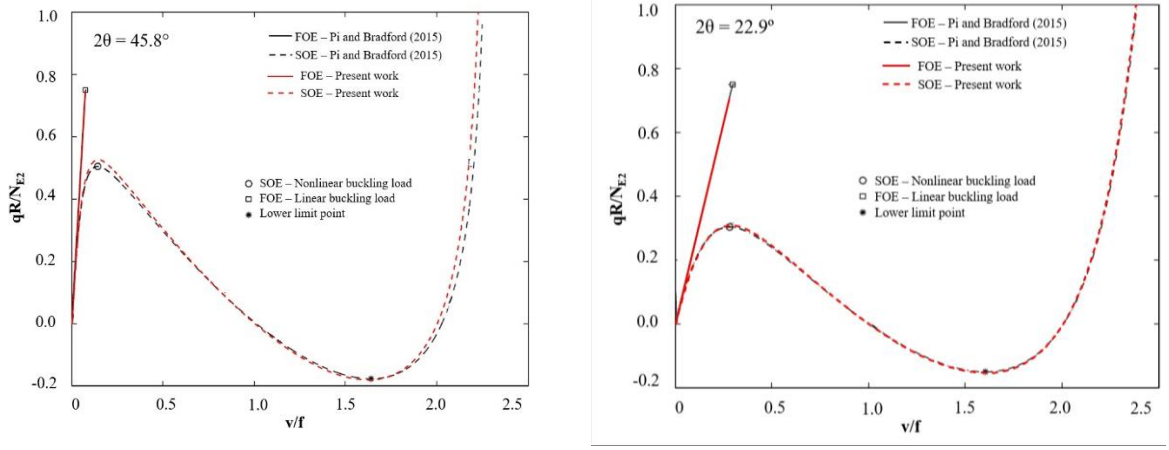

a) 2θ = 45,8° b) 2θ = 22,9°

Figure 2. Three-pinned arch equilibrium paths

4 Parametric study

In this section, the geometric and physical parameters influence on the structural behavior of the three-pinned arch are verified. Changes in model geometry, modulus of elasticity, yield stress, arch shape and boundary conditions are considered.

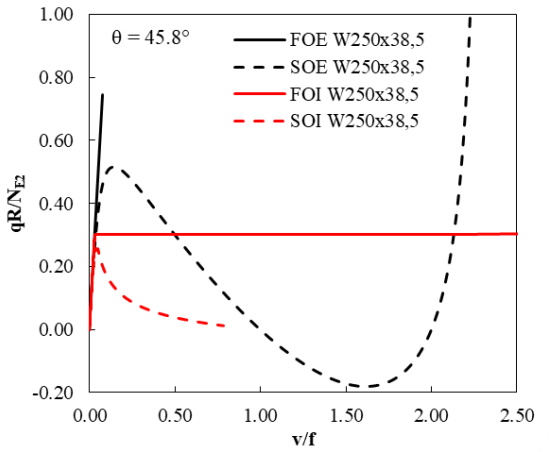

Figure 3. Three-pinned arch equilibrium paths: FOE, SOE, FOI, and SOI

4.1 Influence of model geometry

To verify the influence of the model geometric parameters, SOE and SOI analyses were performed. Table 2 presents the geometric data for the profiles cross-section, while Tab. 3 presents the information related to the geometry, material and loads of the models. It should also be noted that the values for the applied load were defined according to Eq. (6), varying according to the modulus of elasticity and second moment of inertia.

Table 2. Profiles cross-section geometric properties

Shape	**A (mm²)**	**Izz (mm⁴)**	**Iyy (mm⁴)**	**J (mm⁴)**	**Cw (mm6)**	**Zzz (mm³)**	**Zyy (mm³)**
W200X15	1910	1.28E+07	872000	17700	8.31E+09	145000	27200
W200X31,3	3980	3.13E+07	4.07E+06	117000	4.08E+10	334000	93200
W250X38,5	4910	6.00E+07	5.87E+06	167000	9.26E+10	512000	123000
W250X58	7400	8.70E+07	1.87E+07	406000	2.66E+11	768000	281000
W310X79	10000	1.77E+08	3.99E+07	657000	8.49E+11	1,28E+06	478000

Table 3. Geometry, material and loading data

Shape	**E (kN/mm²)**	**2θ (°)**	**Radius (R) (mm)**	**Arch Lenght (S) (mm)**	**N_{E2} (kN)**	**fy (kN/mm²)**	**q (kN/mm)**
W200X15	200	45.8	13510.79	10800	866.4673	0.25	0.0641315
W200X31.3					2118.783		0.1568215
W250X38.5					4061.566		0.3006163
W250X58					5889.27		0.4358937
W310X79					11981.62		0.8868182

Figure 4a shows the equilibrium paths for the different arch profiles considering the SOE. Observe the similarity of the curves and that the limit points differences are associated to the dependence that the applied load on the value of the second moment of inertia. Similar behavior can be observed for the SOI analyses (Fig. 4b). Table 4 presents the elastic and inelastic critical load for each profile.

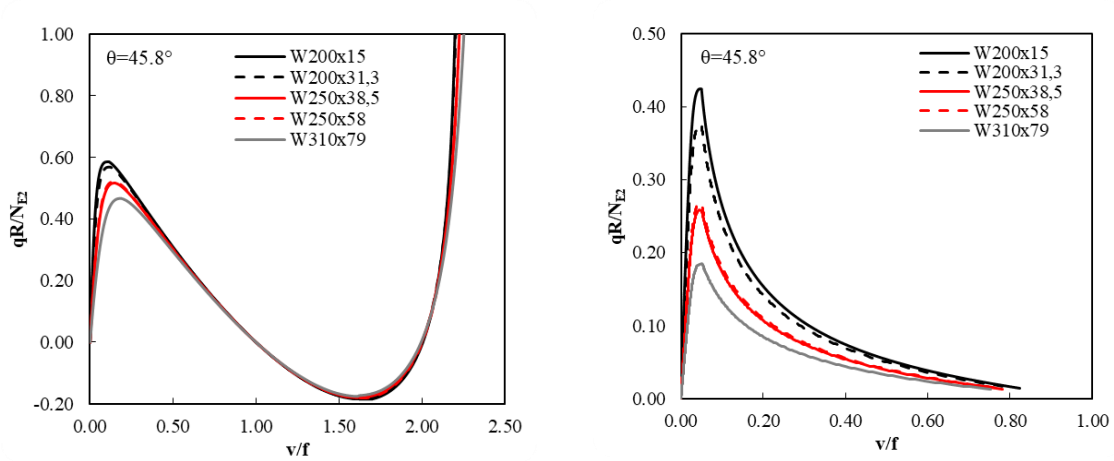

a) SOE b) SOI

Figure 4. Equilibrium paths for various three-pinned arch profiles

Table 4. Three-pinned arch critical loads – SOE and SOI for various profiles

Perfis	**qR/N_{E2} (cr) (SOE)**	**qR/N_{E2} (cr) (SOI)**
W200X15	0.584	0.4240
W200X31.3	0.569	0.3750
W250X38.5	0.517	0.2580
W250X58	0.522	0.2670
W310X79	0.467	0.1849

4.2 Young's modulus variation

To verify the influence of the Young's modulus, SOE and SOI analyses were performed, but only the SOI results are shown in Fig. 5. Table 5 reproduces the limit load values for both analyses. The SOE results show the same limit load value for different Young's modulus values, which is explained by the direct dependence that radial load has on the Young's modulus. This is not observed for the SOI analyses, justified by the consideration of physical nonlinearity. In this case, as the modulus of elasticity increases, the critical load is smaller because the applied radial load is greater.

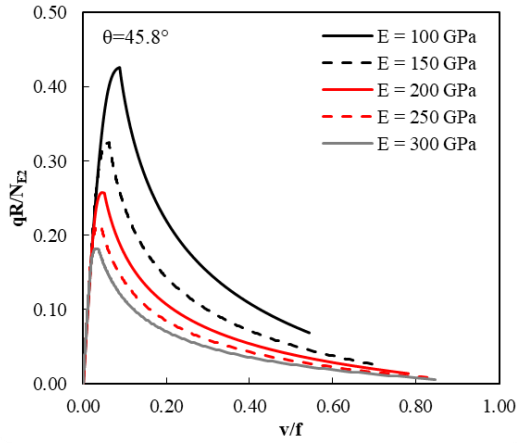

Figure 5. Three-pinned equilibrium paths – SOI: Young's modulus variation

Table 5. Three-pinned critical loads – SOE and SOI for various Young's modulus

E (GPa)	qR/N_{E2} (cr) (SOE)	qR/N_{E2} (cr) (SOI)
100	0.517	0.426
150	0.517	0.325
200	0.517	0.258
250	0.517	0.214
300	0.517	0.182

4.3 Influence of yielding stress

Only SOI analyses were made to verify the influence of the yield stress fy, whose equilibrium paths can be seen in Fig. 6 and the critical loads values in Tab. 6. Evaluating these results, it is observed that as it increases the material yield stress value, the critical load value also increases, describing an expected behavior.

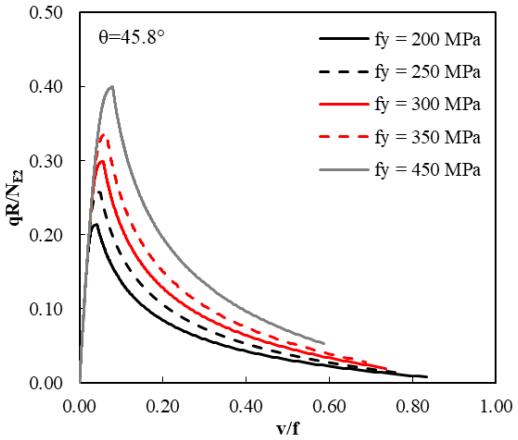

Figure 6. Three-pinned arch equilibrium paths – SOI for various yield stress

Tabela 6. Three-pinned arch critical load – ISO for various yield stress

fy (MPa)	qR/N_{E2} (cr) (SOI)
200	0.214
250	0.258
300	0.299
350	0.337
450	0.400

4.4 Influence of arch shape configurations

Another influencing parameter studied in this research is the variation in the arch shape. This is made here varying the angle of the arch (consequently the height of its focus) and keeping its length constant in all analyses. The equilibrium paths obtained for SOE and SOI analyses can be seen in Figs. 7 and 8, respectively. There is a similar behavior for the equilibrium paths, with the arch increasing its resistance as the focus increases.

4.5 Influence of arch boundary conditions

Finally, this research brings a study related to the influence of boundary conditions on the arch behavior. SOE and SOI analyses were carryout considering the complete arch geometry (FA) to allow combinations of the support condition, and $2\theta = 45{,}8^{o}$. The equilibrium paths are shown in Fig. 9 and show similar structural behavior for the different boundary conditions. However, with the SOE analysis, it is possible to see that the increase in the

degree of fixation increases the rigidity of the model. The structural behavior for the SOI analyses is similar, but due to the forces redistribution for the pinned-pinned condition, it is possible to obtain a post-critical response.

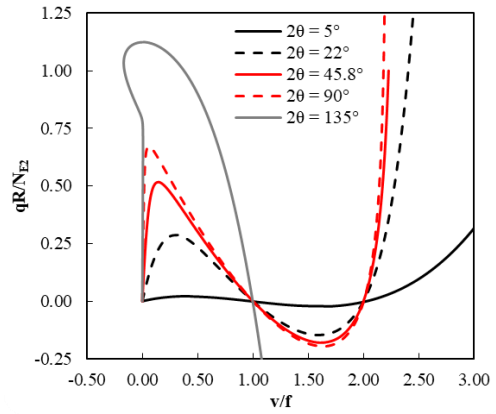

Figure 7. Three-pined arch equilibrium paths – SOE for arch shape variations

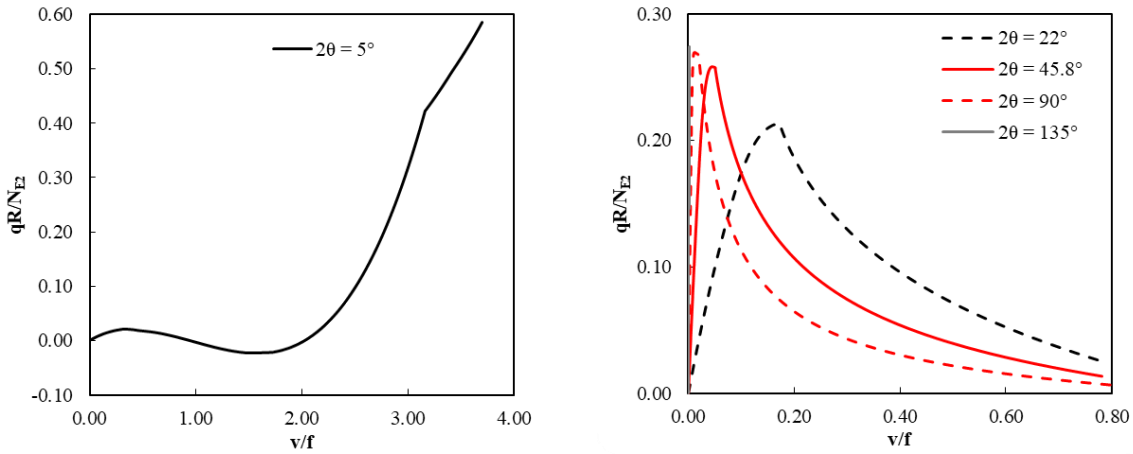

Figure 8. Three-pined arch equilibrium paths – SOI for arch shape variations

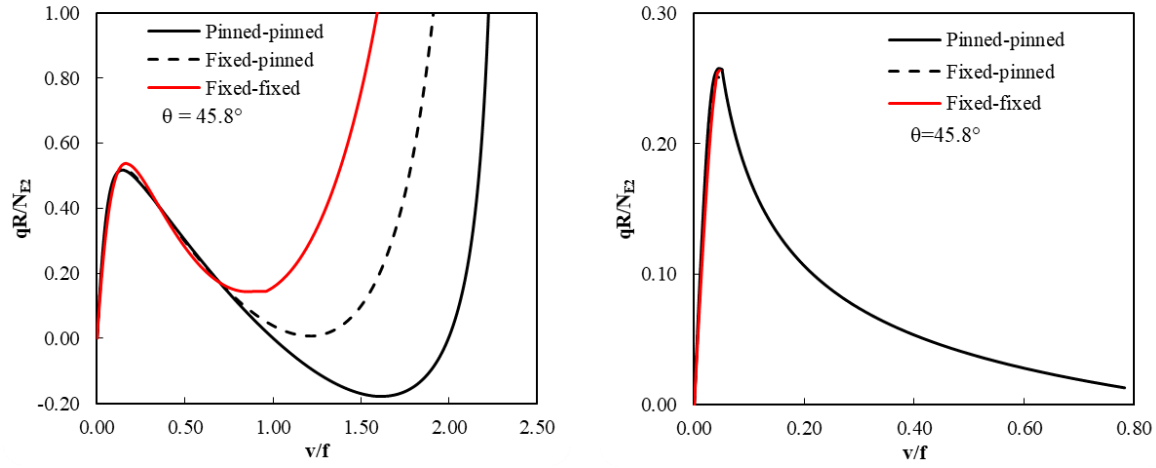

a) SOE b) SOI

Figure 9. Arch equilibrium paths: SOE and SOI for boundary condition variation

5 Final comments

This study aimed to evaluate the structural behavior of three-pinned arches through numerical modeling using the finite element method. To perform the first and second-order elastic and inelastic analyses, the MASTAN2 software was used, which are in accordance with the results available in literature.

The three-pinned arches analysed, as expected, showed a strongly non-linear behavior, highlighting the importance of taking these effects into account. It was possible to determine the importance that the studied parameters have in the arches' structural behavior. With this study, it was possible to predict the configurations that allow the arch to gain strength and stiffness.

Acknowledgements. This numerical study was made with the support from CAPES, CNPq, FAPEMIG, PROPEC and PROPPI/UFOP. The authors also thank the prof. Ronald Ziemian for the availability of MASTAN2.

Authorship statement. The authors hereby confirm that they are the solely liable persons responsible for the authorship of this study, and that all material that has been herein included as part of the present article is either the property (and authorship) of the authors, or has the permission of the owners to be included herein.

References

[1] Ziemian R., McGuire W. Mastan2 V3.0.7 2006.

[2] Prado I. CS-ASA Preprocessor: Sistema Gráfico Interativo de Pré-processamento para Análise Avançada de Estruturas. Master's Dissertation in Civil Engineering. Ouro Preto, MG, Brazil: Programa de Pós-Graduação em Engenharia Civil, Deciv/EM/UFOP; 2012.

[3] McGuire W, Gallagher RH, Ziemian RD. Matrix Structural Analysis. 2nd Editio. Copyright by Ronald D. Ziemian; 2014.

[4] Pi Y-L, Bradford MA. In-Plane Analyses of Elastic Three-Pinned Steel Arches. J Struct Eng 2015;141:06014009. https://doi.org/10.1061/(ASCE)ST.1943-541X.0001135.